Atmospheric Chemistry and Physics

Biogenic nitrogen oxide emissions from soils: impact on NO_x and ozone over west Africa during AMMA (African Monsoon Multidisciplinary Analysis): observational study

D. J. Stewart[1], C. M. Taylor[2], C. E. Reeves[1], and J. B. McQuaid[3]

[1]School of Environmental Sciences, UEA, Norwich, UK
[2]Centre for Ecology and Hydrology, Wallingford, UK
[3]School of the Environment, University of Leeds, UK

Abstract. Chemical and meteorological parameters measured on board the Facility for Airborne Atmospheric Measurements (FAAM) BAe 146 Atmospheric Research Aircraft during the African Monsoon Multidisciplinary Analysis (AMMA) campaign are presented to show the impact of NO_x emissions from recently wetted soils in West Africa. NO emissions from soils have been previously observed in many geographical areas with different types of soil/vegetation cover during small scale studies and have been inferred at large scales from satellite measurements of NO_x. This study is the first dedicated to showing the emissions of NO_x at an intermediate scale between local surface sites and continental satellite measurements. The measurements reveal pronounced mesoscale variations in NO_x concentrations closely linked to spatial patterns of antecedent rainfall. Fluxes required to maintain the NO_x concentrations observed by the BAe-146 in a number of cases studies and for a range of assumed OH concentrations (1×10^6 to 1×10^7 molecules cm^{-3}) are calculated to be in the range 8.4 to 36.1 ng N m^{-2} s^{-1}. These values are comparable to the range of fluxes from 0.5 to 28 ng N m^{-2} s^{-1} reported from small scale field studies in a variety of non-nutrient rich tropical and sub-tropical locations reported in the review of Davidson and Kingerlee (1997). The fluxes calculated in the present study have been scaled up to cover the area of the Sahel bounded by 10 to 20 N and 10 E to 20 W giving an estimated emission of 0.03 to 0.30 Tg N from this area for

July and August 2006. The observed chemical data also suggest that the NO_x emitted from soils is taking part in ozone formation as ozone concentrations exhibit similar fine scale structure to the NO_x, with enhancements over the wet soils. Such variability can not be explained on the basis of transport from other areas.

Delon et al. (2008) is a companion paper to this one which models the impact of soil NO_x emissions on the NO_x and ozone concentration over West Africa during AMMA. It employs an artificial neural network to define the emissions of NO_x from soils, integrated into a coupled chemistry-dynamics model. The results are compared to the observed data presented in this paper. Here we compare fluxes deduced from the observed data with the model-derived values from Delon et al. (2008).

1 Introduction

Oxides of nitrogen play a key role in almost all aspects of atmospheric chemistry.

Emissions of nitrogen oxides ($NO_x=NO+NO_2$) are a key factor in tropospheric ozone production and affect the oxidative capacity of the atmosphere (Wayne, 1991). Due to the influence they have on aerosol composition and ozone formation, NO_x emissions may also have an impact on the radiative balance of the atmosphere (Prather and Enhalt, 2001).

In rural, tropical regions the main source of ground level NO_x in the dry season is anthropogenic – mainly due to human-initiated fires. There is also evidence from satellite data in the Sahel that emissions of NO from wet soils in the

rainy season may lead to a significant enhancement of NO$_x$ in the region (Jaegle et al., 2004). This is supported by field and laboratory measurements which report very low fluxes during the dry season (Levine et al., 1996; Scholes et al., 1997) and large NO pulses when the soils of dry savannahs or seasonally dry forests are exposed to rainfall (Johannsson and Sanhueza, 1988; Davidson, 1992; Harris et al., 1996; Levine et al., 1996; Kirkman et al., 2001; Scholes et al., 1997; Serça et al., 1998). Following the initial rapid pulse after wetting enhanced NO emission persists for a number of days (Hall et al., 1996), with sandy soils drying out and the NO emission falling to "background" levels in the order of 2–3 days (Johannsson et al., 1988; Scholes et al., 1997). If rainfall events are frequent enough NO emissions remain elevated for the whole of the rainy season.

Global estimates of NO$_x$ sources show that biogenic emissions of NO$_x$ from soils are significant, accounting for 14% of tropospheric NO$_x$ (Delmas et al., 1997). Tropical soils contribute up to 70% of the total global soil emissions (Yienger and Levy, 1995), with model studies showing that Africa accounts for 30% of these tropical emissions (Jaegle et al., 2005). It is believed that these NO emissions are caused by microbes in the soil that are water-stressed and remain dormant in dry periods The microbes are activated by the first rainfall of the season and metabolise accumulated nitrogen (as ammonium and nitrate ions) in the soil leading to NO as one of the by-products, which is then emitted into the atmosphere (Hall et al., 1996; Delmas et al., 1997). Although emissions from soils are in the form of NO (Conrad, 1996), once in the atmosphere NO is rapidly converted to NO$_2$ by reaction with ozone. Some of this NO$_2$ can subsequently be photolysed back to NO and through this cycle of reactions a photostationary state between NO-NO$_2$ and ozone can be established. Therefore in this paper concentrations of NO$_x$ are used to quantify the amount of NO emitted from the soil.

The current estimates of the amount of NO$_x$ produced from tropical soils in this way are poorly constrained due to lack of relevant field measurements and the temporal and spatial heterogeneities in pH, soil temperature, soil type and soil moisture content. In fact, published estimates differ by a factor of 4 (5–21 Tg N/yr) (Davidson and Kingerlee, 1997; Delmas et al., 1997; Davidson, 1991; Watson et al., 1992; Potter et al., 1996; Yienger and Levy, 1995). Jaegle et al. (2004) infer from satellite measurements of NO$_2$ that the contribution of NO from African soils is 3.3±1.8 Tg N/yr, and extrapolating this to cover all the tropics they estimate a global contribution of 7.3 Tg N/yr from biogenic soil sources.

In this study, data are presented from 3 flights carried out as part of the AMMA (African Monsoon Multidisciplinary Analysis; Redelsperger et al., 2006) campaign which had the aim of relating physical and chemical properties of the daytime boundary layer with soil moisture patterns to the north of Niamey, Niger in July and August 2006. These flights consisted of a series of long low-level transects over arid areas that had experienced rainfall in the previous 1–3 days.

This study is closely associated with the companion paper Delon et al. (2008). Both studies determine fluxes of NO$_x$ from soil over West Africa, which are compared. This paper employs a top-down approach using NO$_x$ concentrations measured in the boundary layer on the BAe-146 aircraft, whilst Delon et al. (2008) employ a bottom-up approach by incorporating an artificial neural network (ANN), constrained by previous field studies, into a 3-D mesoscale, coupled chemistry-dynamics model and comparing the resulting NO$_x$ concentrations with those measured on the BAe-146. In this current study the variation of NO$_x$ and ozone in the boundary layer is examined with respect to the soil moisture, as indicated by the surface temperature anomalies. In Delon et al. (2008), the ability of the model to capture these observed features is examined.

2 Experimental

The gas-phase chemistry measurements discussed in this paper were made on board the FAAM BAe146 Atmospheric Research Aircraft which was based in Niamey, Niger for the AMMA campaign from 17 July to 17 August 2006.

2.1 NO$_x$ instrumentation

NO$_x$ measurements were made using two instruments on board the FAAM BAe 146. The instrument used in all flights was a commercial TECO 42C chemiluminescence NO$_x$ analyser. This is a two channel (NO and NO$_x$) instrument utilising a single chamber and photomultiplier tube in which the chemiluminescence reaction with ozone is used to measure NO. The sample gas passes through a solenoid valve which routes the sample directly to the reaction chamber (NO mode) or through a molybdenum converter which converts NO$_2$ (and some other NO$_y$ species) to NO before entering the chamber (NO$_x$ mode). The limit of detection of the TECO analyser is 50 ppt with a 120 s averaging time with an uncertainty of 1% of full scale (5 ppb). The other instrument was the University of East Anglia (UEA) NO$_{xy}$ which measures NO by chemiluminescence and NO$_2$ by photolytic conversion of NO$_2$ to NO which is measured by chemiluminescence in a second detector. This instrument was operated for 10 flights towards the end of the campaign. Detection limits of the UEA NO$_{xy}$ are of the order of 3 pptv for NO and 15 pptv for NO$_2$ for 10-s data with estimated accuracies of 8% for NO at 1 ppb and 9% for NO$_2$ at 1 ppb. The instrument is described in detail in Brough et al. (2003).

Since the TECO is a less sensitive instrument than the NO$_{xy}$ and may include a fraction of NO$_z$ (NO$_y$-NO$_x$) in its measure of NO$_2$, a comparison between the 2 instruments was performed for the flights when both instruments were operated to evaluate the quality of the TECO data and to determine whether its measurements of NO$_x$ could be used for flights when the NO$_{xy}$ was not operated. Figure 1 shows a
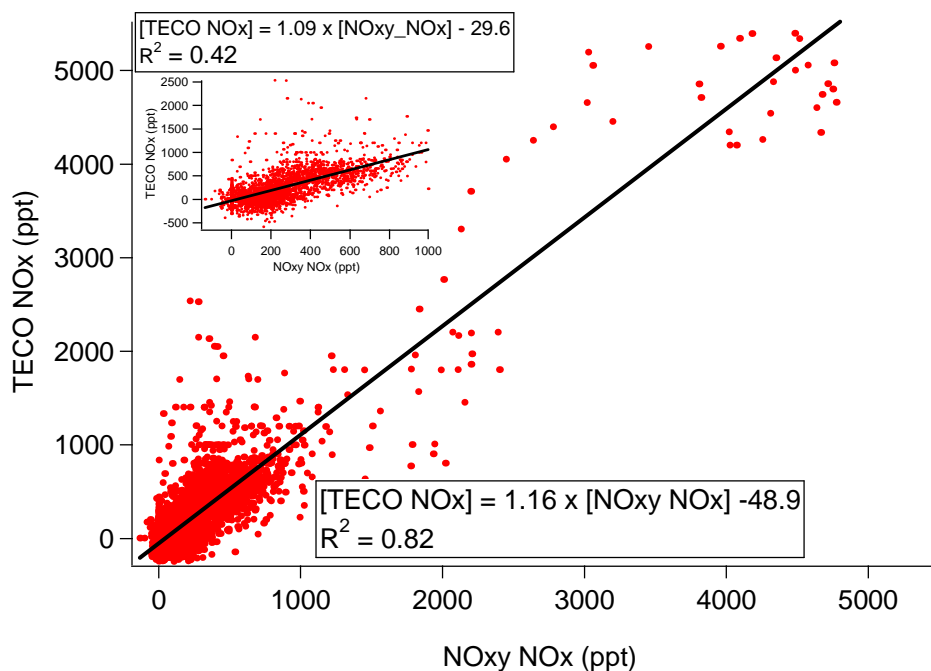
Fig. 1. A scatter plot showing the intercomparison of NO$_x$ data from the TECO and NO$_{xy}$ instruments for all boundary layer data collected throughout the AMMA campaign. Inset shows all data below 1 ppb (as measured by the NO$_{xy}$ instrument).

scatter plot of the 10-s averaged data for all of the data in the boundary layer throughout the AMMA campaign. The boundary layer height was determined from plots of potential temperature vs. altitude calculated either from drop sonde data or in the absence of operational sondes from in situ aircraft data on profile ascents and descents. It is apparent from Fig. 1 that the TECO instrument is reading systematically slightly higher (16%) than the NO$_{xy}$, possibly due to a known NO$_z$ interference, which is discussed in detail in Steinbacher et al. (2007). At NO$_x$ concentrations below 1 ppb (as measured by the UEA NO$_{xy}$) this overestimation is not as pronounced (9% with an uncertainty of 3% based on the standard deviation (1 σ) and 5% based on the 95% confidence interval). In both cases (for all data and data below 1 ppb), the differences in the TECO and NO$_{xy}$ data are close to the estimated accuracies of the NO$_{xy}$ NO and NO$_2$ channel (8% for NO at 1 ppb and 9% for NO$_2$ at 1 ppb giving a combined uncertainty of 12.5% for total NO$_x$ at 1 ppb). The correlation coefficient for all the data in the boundary layer is good at 0.82 but this declines to 0.42 below 1 ppb (as measured by the UEA NO$_{xy}$), demonstrating the relatively high noise in the TECO data at these concentrations. This comparison therefore shows generally good agreement between the two instruments, but also illustrates that caution should be exercised when using TECO data below 1 ppb. Therefore in this study where we are using data with concentrations mostly below 1 ppb, we have been careful to only select cases where we have observed enhancements in NO$_x$ for sustained peri-

ods of several minutes in which errors due to random noise are substantially reduced.

2.2 Other instrumentation

Ozone was measured using a TECO 49C UV photometric instrument. This instrument has been modified with the addition of a drier. The inlet from the port air sample pipe is pumped via a buffer volume to maintain the inlet air at near surface pressure. All surfaces in contact with the sample including the pump are of polytetrafluoroethylene (PTFE) or PFA. The instrument has a range of 0–2000 ppbv, a detection limit of 2 ppbv and a linearity of (5% $\pm$ 2 ppb) (as stated by the manufacturer).

Carbon monoxide was measured by VUV resonance fluorescence using an Aero Laser AL5002 Fast Carbon Monoxide (CO) Monitor. With an integration time of 10 s the detection limit is <2.0 ppbv. The measurement technique is described in detail in Gerbig et al. (1999).

Acetonitrile and benzene were measured using a Proton Transfer Mass Spectrometer (PTrMS) supplied by Ionicon Analytik to which slight modifications have been made. The technique is based on the transfer of a proton from H$_3$O$^+$ to organic compounds which have a higher proton affinity. The resulting ions are then detected using mass spectrometry. The instrument was operated using a cycle in which the mass spectrometer scans over a mass range resulting in a point measurement for each species of interest approximately every 15 s.
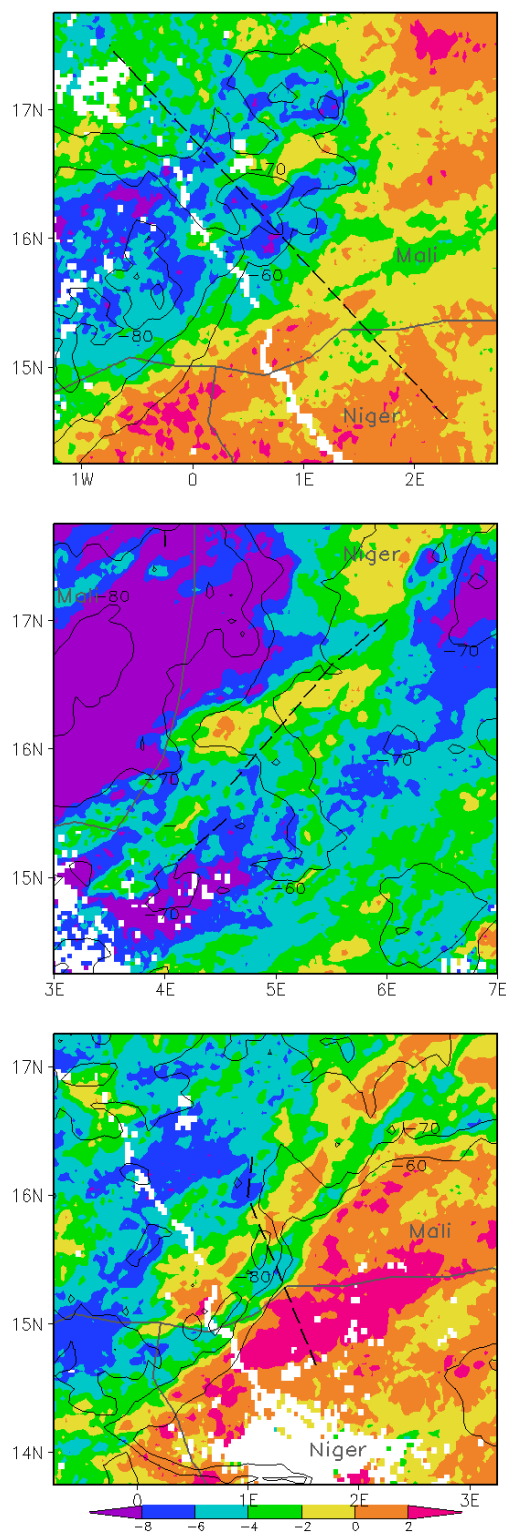
Fig. 2. LSTA (K) maps (shaded) for flights described in the case studies with the low level flight tracks (dotted line), **(a)** B224, **(b)** B227 and **(c)** B217. White denotes no data due to cloud cover or water bodies. The contours indicate minimum cold cloud temperature during the previous storms.

PAN was measured using a two channel gas chromatograph with fused silica capillary columns coupled with electron capture detection. The use of two channels doubled the frequency of the PAN measurement and provided data every 90 s with a detection limit of ∼30 ppt (S/N=3).

2.3 Flight planning

Rainfall in the Sahel is intermittent in space and time. The top layers of the soil usually have time to dry out between storms, which have typical return times of 3 days during the rainy season. Fluxes of NO are very strong within a few hours after rain but decrease rapidly on the second and third days (Sanhueza, 1992; Levine, 1993) while evaporation (sensible heat flux) remains relatively high (low) (Taylor et al., 1997). During the wet season, rainfall therefore produces a highly heterogeneous and evolving surface, with strong contrasts in physical and chemical fluxes into the atmosphere dependant on local antecedent rainfall.

The aim of the flights presented here was to characterise the physical and chemical response of the boundary layer to the complex surface forcing following rain. Flight tracks were designed to cross regions where soil moisture contrasts were large due to the passage of storms across part of the track. This was possible through the combined use of cold cloud top temperature imagery during the storms (from Meteosat) to track likely precipitating systems, supplemented by more accurate mapping of wet and dry surfaces using land surface temperature (LST) data from Meteosat on the morning of the flight. Anomalies were computed from the longer term mean diurnal cycle of LST for each pixel for every cloud-free slot. The LST data were downloaded in near-real time from LandSAF (http://landsaf.meteo.pt/) and a daytime average (07:00 to 17:00 UTC) map of LST anomaly (LSTA) data from all 41 slots was used to characterise soil moisture gradients on the day of the flight, based on the principle that when a soil is wetted, it is cooler than more typical, drier conditions (e.g. Taylor et al., 2003).

3 Results and discussion

In this section, 3 case studies are presented which illustrate the spatial relationships observed between soil moisture (inferred from LSTA) and the various physical and chemical parameters in the boundary layer. Subsequently fluxes of NO$_x$ from wet soils are calculated from concentration data on 5 flights to determine the typical strength of this source. These estimates are compared to other literature values, and discussed in terms of their regional significance.

The tracks of the three case studies are shown in Fig. 2, overlaid on maps of LSTA for that day. These cases were selected from the larger series of AMMA flights because they captured well-defined soil moisture features which were detectable with LSTA due to lack of cloud. In addition, the
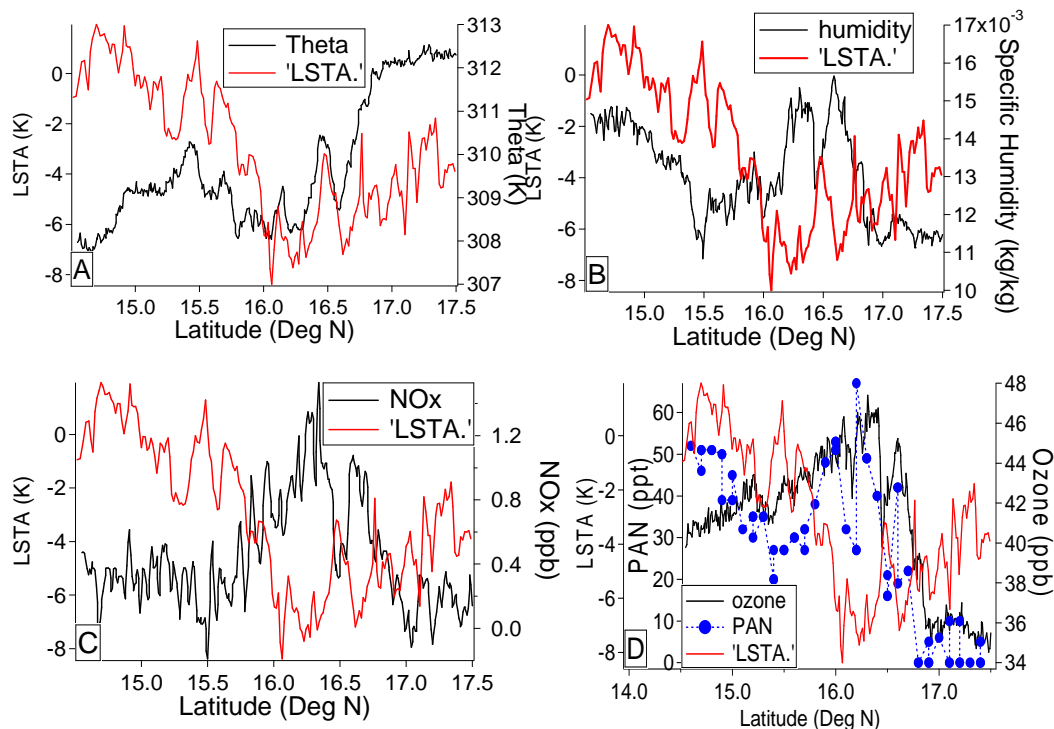
Fig. 3. The variation of LSTA and **(a)** potential temperature, **(b)** specific humidity, **(c)** TECO NO$_x$, and **(d)** ozone and PAN as a function of latitude during a low level transect over wet features (as described in the text) for flight B224.

boundary layer structure on these flights was not affected directly by deep convective mixing during or in the hours prior to take-off. All 3 flights took place during the afternoon, when the boundary layer was relatively deep. The vegetation cover on all 3 flights was generally sparse with a seasonal herbaceous layer just starting to emerge between woody coverage of a few percent.

### 3.1 Case study 1: flight B224 – 1 August 2006

The first flight discussed was performed approximately 18 h after a major storm developed in northern Mali around 16 N, 1 E which subsequently travelled south-westwards. The broad track of that storm is evident from the contours of satellite cold cloud (Fig. 2a), whilst the LSTA data provide a higher spatial resolution picture of the resulting pattern of cool (and wet) surfaces adjacent to warmer, drier zones. The aircraft crossed the region roughly perpendicular to the swath of high soil moisture at a height of approximately 170 m. The LSTA map also indicates the effect of other storms on the flight track two and four days prior to the flight. A more detailed history of these storms and the impact of the soil moisture on the physical properties of the boundary layer has been presented by Taylor et al. (2007).

The response of the boundary layer potential temperature and specific humidity to soil moisture along the track is shown in Fig. 3a and b. In sections of the track over-

flying wet soils, as indicated by strongly negative LSTA, the boundary layer was locally cooler and moister, due to the increased latent and reduced sensible heat fluxes from the ground. This effect was most notable on the track above the storm of the previous afternoon, between 16.1 and 16.45 N and again around 16.6 N, though earlier storms also affected the boundary layer between 15 and 16 N. Vertical temperature and humidity profile data (Taylor et al., 2007) also indicate that the boundary layer over the wet soil was typically half the depth of nearby drier regions, due to variations in sensible heat flux. These mesoscale surface-forced features were superimposed on the large-scale meridional gradient of increasing temperature and decreasing specific humidity from south to north.

The chemical response of the boundary layer to the soil moisture features is evident in Fig. 3c and d. There was a striking impact of soil moisture on the NO$_x$ concentration: NO$_x$ exceeded 1 ppb directly above the soil wetted the previous day, whilst the measured concentration fell sharply when the aircraft flew over adjacent drier soil (e.g. at 16.5 N). An anthropogenic source of this NO$_x$ can be ruled out as NO$_x$ and CO are very poorly correlated (R^2=0.04). Unfortunately the PTr-MS was not operated on this flight so no correlations between NO$_x$ and benzene or acetonitrile can be presented.

Over the wet soil features the concentrations of ozone were also enhanced from 36 to 47 ppb with fine scale structure associated with the wet and dry regions as shown in
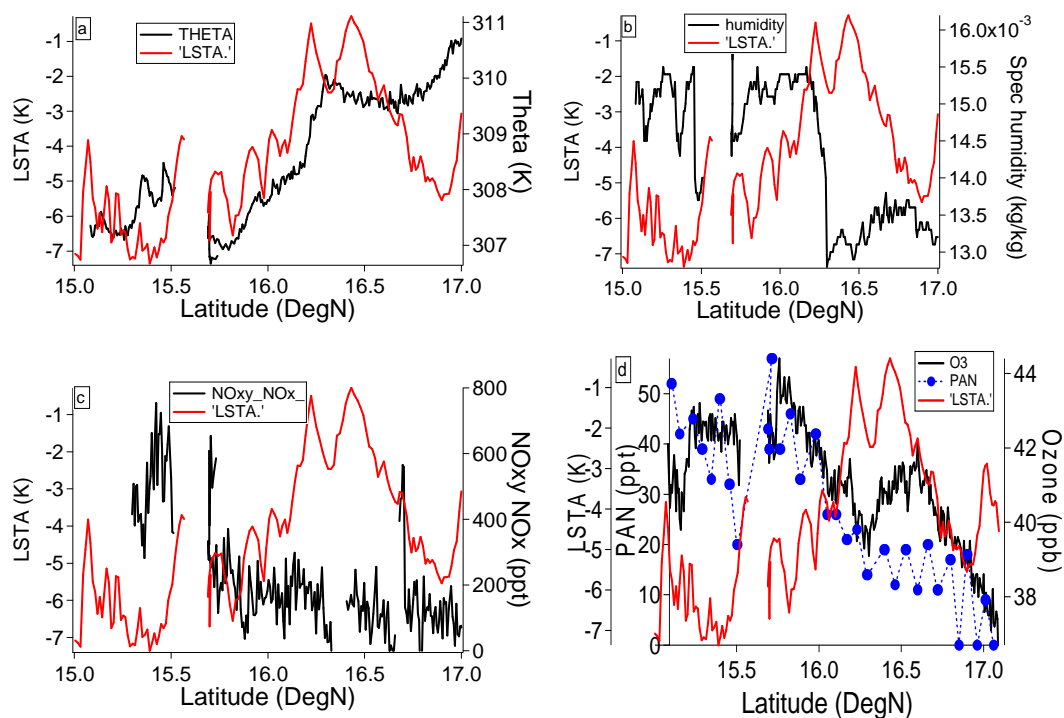
Fig. 4. The variation of LSTA with **(a)** potential temperature, **(b)** specific humidity, **(c)** NO$_{xy}$ NO$_x$ and **(d)** ozone and PAN as a function of latitude during a low level transect over wet features (as described in the text) for flight B227.

Fig. 3d. The lower values of ozone were comparable with data taken at either end of the transect above the boundary layer, and imply the maxima were confined to the boundary layer. These features are consistent with local production of ozone over the wet soils driven by NO$_x$ emissions. Further evidence of photochemical ozone production is available from the PAN (peroxyacetyl nitrate) data which correlates well with the NO$_x$ and ozone increasing from around 20 ppt where NO$_x$ and ozone are low up to 70 ppt in the region where NO$_x$ and ozone are enhanced (Fig. 3d).

3.2 Case study 2: flight B227 – 6 August 2006

This flight was designed to sample mesoscale soil moisture features produced by rainfall on the previous afternoon and overnight on a transect to the north-east of Niamey and over a desert region to the west of the Aïr Mountains (Fig. 2b) and is the focus of the study by Delon et al. (2008). The surface was wetted near the northern end of the transect (around 17 N, 7 E) and, in patches, on the flight track south of approximately 16.2 N. In both of these areas, LSTA was −6 K or cooler. In the region between 16.2 and 17.0 N, patches of moderately negative values of LSTA data were retrieved from satellite, and these patterns were related to an earlier rain event, on the 3–4 August. Because of the presence of dust and the associated poor visibility, the aircraft was unable to descend into the boundary layer overlying the wet zone north of 17 N.

Figure 4 presents boundary layer data from a pair of NE-SW transects over a surface which in the north had largely dried out, but in the south had been wetted in the early hours of that morning. As in the previous case, mesoscale variations in boundary layer temperature and humidity could be linked with changes in surface wetness. In particular, in the region affected by overnight rain south of 16.2 N, the boundary layer was markedly cooler and moister than to the north, though fine scale features were embedded within this structure.

The highest NO$_x$ levels were encountered near areas in the south with an LSTA of typically −6 K. By contrast, low values of LSTA further north (e.g. around 16.9 N) were not associated with local maxima in NO$_x$ concentration. These zones were affected by rain 2–3 days earlier and weak signals of variability in LSTA were evident in atmospheric temperature and humidity data. This is consistent with a weak impact of that storm on heat and water fluxes which persisted for 2–3 days. The lack of a NO$_x$ signal there implies that surface emission decayed more rapidly than evaporation as the soil dried. Similar behaviour was also found over "old" wet zones on flight B224. Again, the fact that the NO$_x$ enhancements observed during this flight are not well correlated with enhancements in CO (R^2=0.23), benzene (R^2=0.01) or acetonitrile (R^2=0.01) rules out an anthropogenic or biomass burning NO$_x$ source. This argument is strengthened when it is considered that a lot of the benzene data was below the 34 ppt detection limit of the PTrMS. Finally, elevated levels
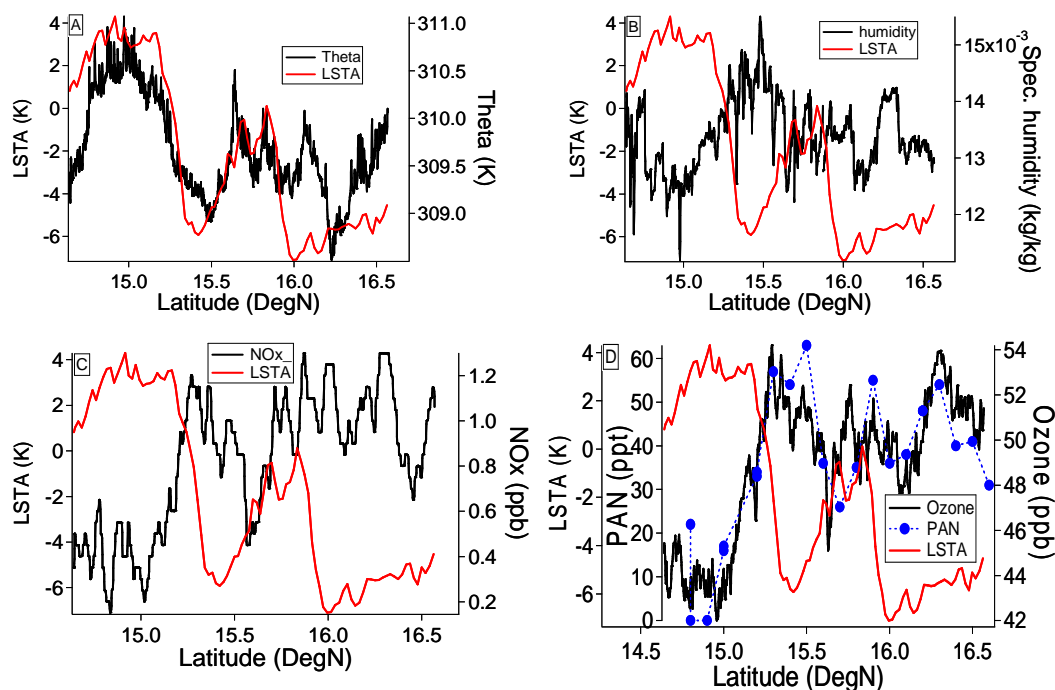
Fig. 5. The variation of LSTA with **(a)** potential temperature, **(b)** specific humidity, **(c)** TECO NO$_x$ and **(d)** ozone and PAN as a function of latitude during a low level transect over wet features (as described in the text) for flight B217.

of ozone (up from 39 ppb to 44 ppb) were also observed on the southerly part of the low level runs occurring over areas of significantly negative LSTA. PAN was also elevated in the areas where higher ozone levels were observed, which is good evidence for photochemical ozone production driven by the NO$_x$ emissions from the soil.

3.3 Case study 3: flight B217 – 21 July 2006

In this case, the aircraft flew to the north of Niamey over 2 well-defined wet zones produced by overnight rain (Fig. 2c). As in the previous two cases, the LSTA correlates very well with the physical properties of the boundary layer on a long low level transect (Fig. 5a and b). The chemical data (NO$_x$, ozone and PAN) also exhibit similar structure to the LSTA (and hence soil moisture) as shown in Fig. 5c and d. The elevations of NO$_x$ are again unlikely to be due to anthropogenic pollution or biomass burning as they are anti-correlated with CO (R^2=0.49) and poorly correlated with acetonitrile (R^2=0.02). No correlation is given for benzene, which was below the instrument detection limit of 29 ppt for almost all of this flight. Such low benzene concentrations in themselves also imply an absence of anthropogenic pollution sources.

The chemical data from this flight exhibit common features with the other 2 cases discussed; strong spatial variability in NO$_x$, ozone and PAN with maxima recorded above wet soils. These cases provide a picture of highly heterogeneous

NO$_x$ emission linked to antecedent rainfall, leading to photochemical ozone production. The issue of ozone production is returned to in Sect. 3.7.

3.4 Flux calculations

In this paper two approaches are used to calculate the NO flux from soils. The first is a time dependent method which calculates the flux required to increase the NO$_x$ from the background concentrations over the surrounding dry soil to the elevated concentrations observed over the wet soils. The second method uses a steady state approach and calculates the flux required to maintain the NO$_x$ concentration observed over the soils. These two methods each have their own advantages, the steady state approach works best for cases when the OH concentration is high and the steady-state conditions are achieved relatively quickly. This method also allows the calculation of an NO flux from the dry soils. For low OH concentrations the time-dependent method is the best approach as NO$_x$ is far from steady-state under these conditions.

3.4.1 Time dependent method

NO$_x$ fluxes have been calculated from the data over areas of the flight track that had received recent rainfall based on the following assumptions: a) the measured concentration of NO$_x$ was well mixed throughout the boundary layer, the height of which was estimated from drop sonde data or from

Table 1. Calculated fluxes using both methods described in the text, fluxes are presented as OH=1×10^6; OH=5×10^6; OH=1×10^7 cm^{-3}.

Flight/Date	BL height (m)	C (TECO) (ppt)	C (NO$_{xy}$) (ppt)	Δt h	SS flux (TECO) ng N m^{-2} s^{-1}	SS flux (NO$_{xy}$) ng N m^{-2} s^{-1}	Time dependent flux (TECO) ng N m^{-2} s^{-1}	Time dependent flux (NO$_{xy}$) ng N m^{-2} s^{-1}
B216 dry (20/07)	1108	405	–	9.0	3.1; 15.3; 30.5	–	–	–
B216 wet (20/07)	705	1023	–	9.0	4.9; 24.5; 49.1	–	11.2; 27.1; 49.7	–
B217 dry (21/07)	1270	300	–	9.0	2.6; 13.0; 25.9	–	–	–
B217A wet (21/07)	620	1024	–	9.0	4.3; 21.6; 43.2	–	9.9; 23.8; 43.8	–
B217B wet (21/07)	620	900	–	9.2	3.8; 19.0; 38.0	–	8.1; 20.7; 38.4	–
B217C wet (21/07)	620	903	–	9.2	3.8; 19.1; 38.1	–	8.2; 20.8; 38.5	–
B224 dry (01/08)	1465	200	–	8.0	2.0; 10.0; 19.9	–	–	–
B224A wet (01/08)	545	918	–	8.0	3.4; 17.0; 34.1	–	10.7; 21.6; 37.8	–
B224B wet (01/08)	545	920	–	8.0	3.4; 17.1; 34.1	–	10.8; 21.7; 37.9	–
B227 dry (06/08)	1300	100	90	10.0	0.9; 4.4; 8.8	0.8; 4.0; 8.0	–	–
B227 wet (06/08)	850	636	600	10.0	3.7; 18.4; 36.8	3.5; 17.4; 34.7	9.5; 20.4; 37.2	9.0; 19.3; 35.1
B230 dry (11/08)	1100	210	210	8.8	1.6; 7.9; 15.7	1.6; 7.9; 15.7	–	–
B230A wet (11/08)	800	746	548	8.8	4.1; 20.3; 40.6	3.0; 14.9; 29.8	10.5; 23.0; 41.3	7.0; 16.6; 30.3
B230B wet (11/08)	800	495	229	9.2	2.7; 13.5; 27.0*	1.2; 6.2; 12.5*	5.9; 14.7; 27.3*	1.4; 6.3; 12.5*
B230C wet (11/08)	800	610	561	9.6	3.3; 16.6; 33.2	3.1; 15.3; 30.5	7.6; 18.2; 33.6	6.8; 16.7; 30.8
B230D wet (11/08)	800	477	520	9.9	2.6; 13.0; 26.0	2.8; 14.2; 28.3	5.3; 13.9; 26.2	6.0; 15.4; 28.6
B230E wet (11/08)	800	471	470	10.4	2.6; 12.8; 25.6	2.6; 12.8; 25.6	5.1; 13.7; 25.8	5.1; 13.7; 25.8

* signifies data not used in calculation of average fluxes – see text for details.

in situ data obtained from the aircraft during profile ascents and descents. Some support for this assumption is drawn from the work of Taylor et al. (2007) who present data from dropsondes from the aircraft for B224. This data shows very little variation in potential temperature and humidity mixing ratio throughout the boundary layer; b) the NO$_x$ was emitted at a constant rate from the time of sunrise to the time of the flight; c) that no significant advection of NO$_x$ into or away from the area of the wet features took place after sunrise; and d) the only NO$_x$ loss processes occurring were deposition to the surface and reaction of NO$_2$ with OH – entrainment losses at the inversion are neglected. The time since sunrise was used to integrate the fluxes over, as strong monsoon winds overnight are likely to remove significant accumulations of locally produced NO$_x$ by dawn. In these calculations the sunrise times were obtained from the StarDate website (www.stardate.org). The NO$_x$ concentrations over dry soil were taken as the average NO$_x$ concentration over regions of dry soil in the boundary layer adjacent to the wet patches. The NO$_x$ concentrations over the wet soils are the average NO$_x$ concentrations measured over wet areas that show a clear elevation above the background "dry" NO$_x$. These assumptions are simplifications, not least the neglect of horizontal and vertical mixing of NO$_x$, which will be significant at the length scales analysed here. A more realistic mixing assumption would increase the flux required to maintain the observed concentrations. The change in concentration with time of a species (C) is given by:

$$\frac{\partial C}{\partial t} = P - LC \tag{1}$$

where P is the production rate of the species and L its loss rate. The solution to this equation is:

$$C_t = C_0 e^{-L\Delta t} + \frac{P}{L}(1 - e^{-L\Delta t}) \tag{2}$$

Assuming that the NO$_x$ is only produced by emission (Flux F, molecules cm^{-2} s^{-1}) of NO from the soil into a boundary layer height of H (cm) and that the concentration over the wet soils at time=0 is the same as that over the dry soils gives:

$$F = \frac{L \cdot \left(C_{wet} - C_{dry} e^{-L\Delta t}\right)}{1 - e^{-L\Delta t}} x H \tag{3}$$

where C_{wet} is the NO$_x$ concentration measured over the wet soil, C_{dry} is the background NO$_x$ concentration measured over the dry soil (in molecules cm^{-3}), L is the loss rate of NO$_x$ in s^{-1}. This loss rate is calculated as the sum of NO$_x$ loss due to reaction with OH (k=1.19×10^{-11} cm^3 molec^{-1} s^{-1}) and deposition to the surface using a deposition velocity of 9×10^{-2} cm s^{-1} (von Kuhlmann et al., 2003). and Δt is the time since sunrise. The calculated fluxes (after conversion of units to ng N m^2 s^{-1}) are shown in Table 1. The fluxes are calculated using a range of possible OH radical concentrations. This range is based on the OH concentrations measured using the University of Leeds Fluorescence Assay by Gas Expansion (FAGE) instrument (which was not operated on all flights) over the AMMA campaign.

3.4.2 Steady-state method

Fluxes can also be calculated by assuming NO$_x$ is in steady state and the production rate is equal to the loss processes at the time of the measurement using Eq. (4).

$$F = H \times L \times C \qquad (4)$$

The fluxes calculated by this method are also shown in Table 1 after conversion of units to ng N m^{-2} s^{-1}. This method allows the fluxes of NO$_x$ from dry soils to be calculated, which is useful since, although NO$_x$ emissions from soils decline sharply following an initial pulse after wetting, the "dry" soils do continue to emit NO$_x$ during the wet season albeit at a lower rate than soils that have been recently wetted (Davidson and Kingerlee, 1997; Johansson and Sanhueza, 1988; Aranibar et al., 2004; Otter et al., 1999; Meixner et al., 1997).

3.4.3 Comparison of the steady state and time dependent flux calculations

The calculated fluxes using both approaches are shown in Table 1. For a fair comparison between the two calculations the flux calculated using the time dependent method should be compared to the difference between the steady state fluxes required to maintain the NO$_x$ concentrations over the wet and the dry soils as the time dependent approach is a calculation of the flux required to maintain the additional NO$_x$ produced by the recent wetting. If the two calculations are compared this way the difference between the wet and dry steady state fluxes are 16–30% of those calculated using the time dependent approach for the case where OH=1×10^6, for the cases where OH is higher (5×10^6 and 1×10^7) the difference in wet and dry steady state fluxes are 30–75% of those calculated using the time dependent method the differences being higher when the background NO$_x$ concentrations are higher i.e. there seems to be more emission from the drier soils. The better agreement at the higher OH concentrations is to be expected as at the time of the observations these cases are closer to steady-state.

3.4.4 Comparison of the flux calculations using the measurements from the different NO$_x$ instruments

The fluxes calculated using data from the two NO$_x$ instruments agree pretty well with the values generally being different by only ∼10% (as can be seen from Table 1), except in the case where the NO$_x$ concentration was relatively low (i.e. 14.0 N, 3.5 E flight B230) and the case where the TECO significantly overestimated the NO$_x$ concentration (e.g. 15.5 N 4.0 E flight B230). In the latter case (marked * in the table) the PAN levels were of the order of 60 ppt whilst the TECO instrument was overestimating NO$_x$ by around 200 ppt. The cause of this is unclear as NO$_y$ equals the sum of NO$_x$ and PAN for most of this flight, suggesting little interference from other NO$_y$ species.

3.5 Comparison of calculated fluxes to previous measurements

Harris et al. (1996) calculated NO$_x$ fluxes based on the concentration profiles of ozone and NO$_x$. They did this by adopting an ozone deposition velocity of 0.2 cm s^{-1} for ozone over bare soil (Warneck, 1988) and estimating of the downward flux of ozone required to balance the observed concentration difference in ozone in the lowest 100 m of the altitude range of the aircraft profile. Assuming the same eddy diffusivity profile for the upward NO$_x$ flux between the same altitudes, and using the observed concentration profile of NO$_x$, an estimate of the flux required to explain the NO$_x$ concentration gradient can be obtained. Unfortunately the AMMA flights were not planned with this type of analysis in mind and suitable vertical profile data was not collected to carry out such a calculation. Using this analysis they obtained a flux of ∼32 ng N m^{-2} s^{-1} which is comparable to the fluxes obtained in this study assuming chemical loss with OH=1×10^7 molecules cm^{-3}.

The average fluxes (averages over all individual wet patches for a given OH concentration) calculated using the data from the NO$_{xy}$ instrument (6.8 to 30.1 ng N m^{-2} s^{-1} value calculated omitting fluxes marked with * in Table 1 using the time dependent method and 3.0 to 29.8 ng N m^{-2} s^{-1} using the steady state method) are of similar order of magnitude to the values of the mean fluxes of NO from soils (∼0.5 to 28 ng N m^{-2} s^{-1}) reported in the review of Davidson and Kingerlee (1997), for a variety of non-nutrient rich land surface types in Africa and other tropical regions. (Higher fluxes reported in this review for nutrient rich sites have not been included in the comparison as the soils of the Sahel are unlikely to have a high nutrient content, based on data presented in Serça et al. (1998) for soil characteristics in Banizoumbou, Niger.) The average fluxes derived from the TECO data (∼8.8 to 37.3 ng N m^{-2} s^{-1} using the time dependent method, 3.6 to 35.5 ng N m^{-2} s^{-1} using the steady state approach) are higher than those calculated from NO$_{xy}$ data due to higher fluxes calculated for earlier flights where the NO$_{xy}$ was not operated, but they are still of a similar order of magnitude to those reported in other studies. This could be due to the earlier flights being closer to the onset of the rainy season when NO emission is expected to be larger. However, in all cases, there had been a number of significant rainfall events in the weeks prior to the flights, so the observations did not capture the first pulse of the season. The different OH values used lead to a range of fluxes which cover a similar range to those reported in the literature. Figure 6 shows the values calculated in this work compared to a range of literature values. The data from this work is presented in three bars with the first giving the average values from the time dependent calculation and the second and third giving the results from the steady-state calculation. In the calculation of this average the fluxes calculated from the NO$_{xy}$ data are used for the later flights as this is the more reliable instrument (with lower
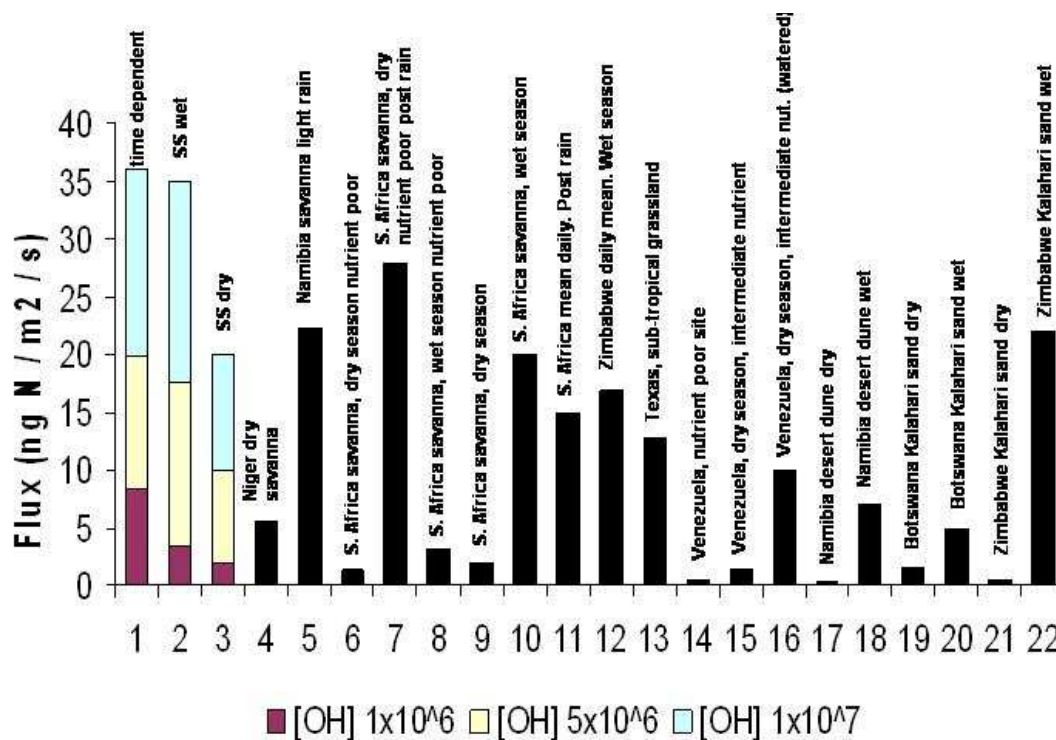
Fig. 6. Average calculated fluxes from AMMA data compared to other fluxes reported in the literature data taken from Davidson and Kingerlee (1997) and Meixner and Yang (2006) and references therein. OH concentrations are in molecules cm^{-3}.

Table 2. Total nitrogen emissions for the region bounded by 10 to 20 N and 10 W to 10 E in July and August 2006 (see text for details).

OH cm^{-3}	Total N emission (TD)[a] (Tg)	Total N emission (SS)[b] (Tg)
1×10^6	0.04	0.03
5×10^6	0.15	0.14
1×10^7	0.30	0.27

[a] (TD) denotes figures derived from analysis of time dependent fluxes
[b] (SS) denotes figures derived from analysis of steady state fluxes

detection limit and better precision) and the TECO data is only used for flights where the NO$_{xy}$ was unavailable. The same rationale has been applied to calculate the average wet and dry steady state fluxes in the second and third columns. The average values obtained in this way are those that will be used in the next section.

The calculated fluxes for flight B227 in this work using the more reliable NO$_{xy}$ instrument (0.8 to 35.1 ng N m^{-2} s^{-1}) are in excellent agreement with the range of fluxes (2 to 35 ng N m^{-2} s^{-1}) calculated using the artificial neural network model of Delon et al. (2008).

3.6 Significance of calculated fluxes

Calculated fluxes for the July/August period were upscaled to the Sahel region from 10 W to 10 E and 10 N to 20 N, an area of 2.3 million km^2. To do this an estimate had to be made the fraction of this area that was recently wetted. This was done using satellite measurements of soil moisture (from AMSR-E). A pixel was judged to be recently wetted when the estimated near surface volumetric soil moisture increased by at least 0.02 m^3 m^{-3} relative to the previous day. This yielded a regional mean wet fraction of 11% during the July/August 2006 period. This "first guess" value can be used as the percentage of the area recently wetted at any given time, assuming that this increase in soil moisture triggers a pulse of NO emissions and that the pulse in emissions last for 24 h. The total amount of nitrogen emitted is then given by the following equations:

$$\text{total N} = (F_{\text{wet}} \times (A \times 0.11) \times t) + (F_{\text{dry}} \times (A \times 0.89) \times t) \quad (5)$$

for the fluxes calculated using the steady state approach and

$$\text{total N} = (F_{\text{wet}} \times (A \times 0.11) \times t) + (F_{\text{dry}} \times (A \times 1) \times t) \quad (6)$$

for the time dependent approach as the wet flux calculated using this method is the additional NO$_x$ produced by recent wetting, where F is the flux of NO in ng N m^{-2} s^{-1}, A is the area of the region in m^2 and t is the length of time considered. The calculated emissions are shown in Table 2

(after conversion of units to Tg N). From this it can be seen that the amount of nitrogen emitted in this region ranges from 0.03 TgN (OH=1×10^6 molecules cm^{-3}) up to 0.30 Tg N (OH=1×10^7 molecules cm^{-3}). There are uncertainties in the values in Table 2, for example the calculation of the area of soil recently wetted and emitting NO at the enhanced rate assumes this enhanced emission to only happen for 24 h after a rainfall event whereas NO pulses have been shown to persist for longer periods. Also the estimate of the area of wet soil may be an underestimate being based on a threshold change between observations which have insufficient temporal resolution to capture the fast dynamics of the top 1 cm of soil.

Jaegle et al. (2004) have estimated a regional contribution of soil emissions to the atmospheric budget of NO_x over Africa in 2000. Using a top down approach from satellite NO_2 data and emissions inventories for fossil and biofuels they obtained an emission from soils of between 0.2 and 0.3 Tg N/month for July and August in north equatorial Africa (0 to 18 N, an area of ~6 million km^2). Using a value of 0.5 Tg N for the sum of soil NO_x emissions for July and August from their analysis and dividing by 2.58 (the ratio of the areas considered) a value of 0.19±0.1 Tg N is obtained (where the error assumes the same 50% value as in their global estimate). As can be seen from Table 2, these values are significantly higher than those calculated in this study (by a factor of 6) at low OH levels but are in reasonable agreement at the higher OH concentrations considered (within 30% for OH=5×10^6 and within 50% for OH=1×10^7, both within the error of the Jaegle estimate). Delon et al. (2008) used an artificial neural network (ANN) model of soil NO emissions coupled with the MesoNH chemistry and transport model to calculate the total amount of nitrogen emitted from soils over the same region for July and August to be 0.024–0.42 Tg N which is in excellent agreement with the value obtained from our simpler upscaling approach. The magnitudes of the amount of nitrogen emitted by this region of the Sahel may be compared to the value of 1.373 Tg N/yr for the entire African continent. However there is evidently much further work required to produce reliable NO_x budgets in this region. The direct comparison of concentration data presented here with satellite column measurements of NO_2 would be a useful next step.

3.7 Evidence of local ozone production over wet soil

In all 3 cases presented, increased NO_x over wet soil is generally accompanied by increased ozone (Figs. 3–5). It is less easy to attribute increased ozone to NO from the wet surface than increased NO_x, due to the relatively long life-time of ozone. Higher ozone in a region could simply reflect transport from a remote source region or from higher in the atmosphere. However, what is striking in the data presented here is the presence of sharp horizontal gradients in boundary layer ozone of up to 6 ppb over 7 km (case 1) and 10 ppb over
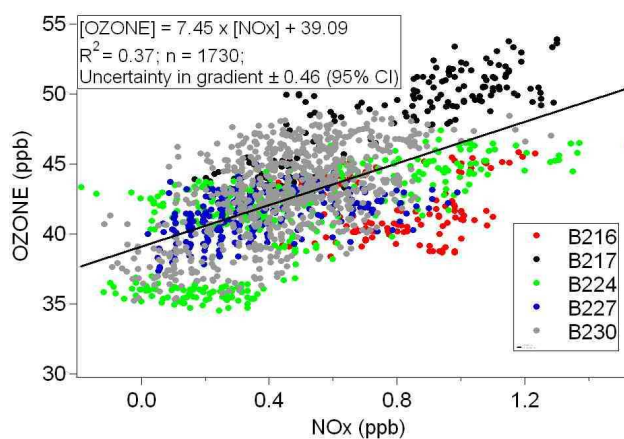
Fig. 7. Scatter plot of TECO NO_x vs. ozone for low level runs from flights in which data is used in Table 1.

40 km (case 3), which are coherent with changes in surface moisture and assumed emission of NO. Transport of ozone from a remote source in a steady flow regime (in this case, the nocturnal monsoon flux) would not maintain such horizontal structure, as turbulent diffusion would dissipate any gradients during the day. Intermittent vertical mixing (by moist convection) could inject an air mass of high ozone (or indeed NO) into the boundary layer which immediately afterwards would be accompanied by sharp horizontal gradients. Again these would dissipate over time. However, there was no evidence of localised convection (from satellite data) in the hours prior to these flights, nor any plausible reason why such mixing would be located over wet soil. In all cases, the deep convection which produced the rainfall, occurred more than 12 h before the data were taken.

The only plausible explanation for the observed spatial variability in ozone is that it resulted from photochemical production in the boundary layer where NO_x concentrations were large. These ozone enhancements were observed 8–10 h after sunrise leading to a possible ozone production rate of the order of 1 ppb h^{-1}. Figure 7 shows good correlation between NO_x and ozone along all the low level transects of the flights where a NO_x flux has been calculated, illustrating the widespread nature of this process. Figure 7 also indicates an ozone production efficiency of 7 molecules of ozone per molecule of NO_x and a background ozone concentration of 40 ppbv. The conclusion of active photochemical production of ozone is also supported by the observations of locally-enhanced PAN above wet soil and the modelling study of Delon et al. (2008). The physical response of the boundary layer to the wet soil would affect the concentration of ozone in several ways. On the one hand, the boundary layer is much shallower over wet, NO-emitting soil, raising concentrations of NO_x and thus the concentration of photochemically produced ozone within the boundary layer. On the other hand, a shallower boundary layer will lead to increased

surface deposition losses of ozone. An impact of the variation in boundary layer depth with soil moisture is that when ozone-rich air moves away from the wet soil, it is mixed into a much deeper ozone-poor boundary layer. If the boundary layer depth were constant, the horizontal ozone gradients surrounding a source would be rather smooth. In this case, where the boundary layer height may double within a few kilometres of the source region, ozone gradients become much larger. Another process acting to enhance horizontal ozone gradients is the development of divergent boundary layer circulations over wet soil patches within drier zones, as identified by Taylor et al. (2007). This increases the residence time of an air parcel over the wet surface during which time ozone may be produced.

4　Conclusions

Elevated levels of NO_x and ozone showing strong spatial variability have been observed during the wet season in a semi-arid region of West Africa during the AMMA 2006 aircraft campaign. These elevations of NO_x correlated well with specific humidity and were anti-correlated with potential temperature and land surface temperature anomalies indicating that the emissions are linked to soil moisture. The elevations in NO_x are not associated with elevated levels of CO, benzene or acetonitrile – ruling out an anthropogenic or biomass burning source for the NO_x. It can, therefore, be confidently stated that the NO_x enhancements are due to emissions from recently wetted soils. Observed NO_x levels over the wet soils (as inferred by the LSTA) are around 0.8–1.4 ppb as compared to background levels of 0–0.2 ppb over dry soils in the same area. To produce the elevated concentrations over wet soils fluxes of $\sim$5.1 to $\sim$11.2 ng N m^{-2} s^{-1} are required if OH is 1×10^6 molecules cm^{-3} or fluxes of up to $\sim$25.6 to $\sim$49.1 ng N m^{-2} s^{-1} with OH concentrations of up to 1×10^7 molecules cm^{-3}. These fluxes are within the range of average NO_x fluxes reported in the literature for a range of tropical and sub-tropical regions in chamber measurements. These calculated fluxes have been scaled up to cover the area of the Sahel bounded by 10 to 20 N and 10 E to 20 W giving an estimated emission of 0.03 to 0.3 Tg N from this area for July and August 2006. This is comparable to the satellite derived estimate of Jaegle et al. (2004), but well within the uncertainties of both calculations. It also compares well with the result derived in the companion paper to this one (Delon et al., 2008) which uses an artificial neural network approach coupled to the MesoNH chemistry and transport model to quantify the total nitrogen flux from this region of the Sahel. Elevations of ozone and PAN were also often observed to be well correlated with the elevations in NO_x and other boundary layer properties suggesting local production of ozone driven by the soil NO_x emissions.

References

Aranibar, J. N., Otter, L., Macko, S. A., Feral, C. J. W., Epstein, H. E., Dowty, P., Eckhardt, F., Shugart, H. H., and Swap, R. J.: Nitrogen cycling in the soil-plant system along a precipitation gradient in the Kalahari sands, Global Change Biol., 10, 359–373, 2004.

Brough N., Reeves, C. E., Penkett, S. A., Stewart, D. J., Dewey, K., Kent, J., Barjat, H., Monks, P. S., Ziereis, H., Stock, P., Huntreiser, H., and Schlager H.: Intercomparison of aircraft instruments on board the C-130 and Falcon 20 over southern Germany during EXPORT 2000, Atmos. Chem. Phys., 3, 1–12, 2003,
http://www.atmos-chem-phys.net/3/1/2003/.

Conrad, R.: Soil microorganisms as controllers of atmospheric trace gases (H$_2$, CO, CH$_4$, OCS, N$_2$O and NO, Microbiological Reviews, 60, 609–640, 1996.

Davidson, E. A.: Fluxes of N$_2$O and NO from terrestrial ecosystems, in: Microbial Production and Consumption of Greenhouse Gases, edited by: Rogers, J. E. and Whitman, W. B., Washington D.C., American Society of Microbiology, 1991.

Davidson, E. A.: Pulses of nitric oxide and nitrous oxide flux following wetting of dry soil: An assessment of probable sources and importance relative to annual fluxes, Ecol. Bull., 42, 149–155, 1992.

Davidson, E. A. and Kingerlee, W.: A global inventory of nitric oxide emissions from soils, Nutr. Cycl. Agroecosys., 48, 37–50, 1997.

Delmas, R., Serça, D., and Jambert, C.: Global inventory of NO_x sources, Nutr. Cycl. Agroecosys. 48, 51–60, 1997.

Delon, C., Reeves, C. E., Stewart, D. J., Serca, D., Dupont, R., Mari, C., Chaboreau, J.-P., and Tulet, P.: Biogenic nitrogen oxide emissions from soils – impact on NO_x and ozone over West Africa during AMMA (African Monsoon Multidisciplinary Experiment): modelling study, Atmos. Chem. Phys., in press, 2008.

Gerbig, C., Schmitgen, S., Kley, D., Volz-Thomas, A., Dewey, K., and Haaks, D.: An improved fast-response vacuum UV resonance fluorescence CO instrument, J. Geophys. Res.-Atmos., 104(D1), 1699–1704, 1999.

Hall, S. J., Matson, P. A., and Roth, P. M.: NO$_x$ emissions from soil: implications for Air Quality Modeling in Agricultural Regions, Ann. Rev. Energ. Env., 21, 311–346, 1996.

Harris, G. W., Wienhold, F. G., and Zenker, T.: Airborne observations of strong biogenic NO$_x$ emissions from the Namibian Savanna at the end of the dry season, J. Geophys. Res.-Atmos., 101, 23 707–23 711, 1996.

Jaegle, L., Martin, R. V., Chance, K., Steinberger, L., Kurosu, T. P., Jacob, D. J., Modi, A. I., Yboué, V., Sigha-Nkamdjou, L., and Galy-Lacaux, C.: Satellite mapping of rain-induced nitric oxide emissions from soils, J. Geophys. Res.-Atmos., 109, D21320, doi:10.1029/2004JD004787, 2004.

Jaegle, L., Steinberger, L., Martin, R. V., and Chance, K.: Global partitioning of NO$_x$ sources using satellite observations: Relative roles of fossil fuel combustion, biomass burning and soil emissions, Faraday Discuss., 130, 407–423, 2005.

Johannsson, C. and Sanhueza, E.: Emission of NO from savanna soils during rainy season, J. Geophys. Res.-Atmos., 93, 14 193–14 198, 1988.

Johannsson, C. Rodhe, H., and Sanhueza, E.: Emission of NO in a tropical savanna and cloud forest during the dry season, J. Geophys. Res.-Atmos., 93, 7180–7192, 1988.

Kirkman, G. A., Yang, W. X., and Meixner, F. X.: Biogenic nitric oxide emissions upscaling: An approach for Zimbabwe, Global Biogeochem. Cycles, 15, 1005–1020, 2001.

von Kuhlmann, R., Lawrence, M. G., Crutzen, P. J., and Rasch, P. J.: A model for studies of tropospheric ozone and nonmethane hydrocarbons: Model description and ozone results, J. Geophys. Res.-Atmos., 108(D9), 4294, doi:10.1029/2002JD002893 2003.

Levine, J. S.: The impact of wetting and burning on biogenic soil emissions of nitric oxide and nitrous oxide in savanna grasslands in S. Africa, paper presented at the 1st International Global Atmospheric Chemistry Symposium, Eilat, Israel, 1993.

Levine, J. S., Winstaed, E. I., and Sebacher, D. I.: Biogenic soil emissions of nitric oxide (NO) and nitrous oxide (N$_2$O) from savannas in South Africa: The impact of wetting and burning, J. Geophys. Res.-Atmos., 101 23 689–23 697, 1996.

Meixner, F. X., Fickinger, Th., Marufu, L., Serça, D., Nathaus, F. J., Makina, E., Mukurumbira, L., and Andreae, M. O.: Preliminary results on nitric oxide emission from a southern African savanna ecosystem, Nut. Cycl. Agroecosys., 48, 123–138, 1997.

Meixner, F. X. and Yang, W. X.: Biogenic Emissions of Nitric Oxide and Nitrous Oxide from Arid and Semi-arid Land, pp. 233–255, in: Dryland Ecohydrology, edited by: D'Odorico, P. and Porporato, A., Springer, Dordrecht Berlin Heidelberg New York, ISBN: 1-4020-4261-2, 2006.

Otter, L. B., Yang, W. X., Scholes, M. C., and Meixner, F. X.: Nitric oxide emissions from a southern African savanna, J. Geophys. Res.-Atmos., 104(D15) 18 471–18 485, 1999.

Potter, C. S., Matson, P. A., Vitousek, P. M., and Davidson, E. A.: Process modelling of controls on nitrogen trace gas emissions from soils world-wide, J. Geophys. Res.-Atmos., 101, 1361–1378, 1996.

Prather, M. and Enhalt, D.: Atmospheric Chemistry and Greenhouse Gases, in: Climate Change 2001: The Science of Climate Change, Chapter 4, pp. 239–287, Cambridge University Press, New York, 2001.

Redelsperger, J. L., Thorncroft, C. D., Diedhiou, A., Lebel, T., Parker, D. J., and Polcher, J.: African Monsoon Multidisciplinary Analysis – An international research project and field campaign, B. Am. Meteorol. Soc., 87, 1739–1746, 2006.

Sanhueza, E.: Biogenic emissions of NO and N$_2$O from tropical savanna soils, paper presented at International Symposium on Global Change, Jpn. Natl. Comm. For the Int. Geosphere-Biosphere Program, Tokyo, 1992.

Scholes, M. C., Martin, R., Scholes, R. J., Parsons, D., and Winstead, E.: NO and N$_2$O emissions from savanna soils following the first simulated rains of the season, Nutr. Cycl. Agroecosys., 48, 115–122, 1997.

Serça, D., Delmas, R., Le Roux, X., Parsons, D. A. B., Scholes, M. C., Abbadie, L., Lensi, R., Ronce, O., and Labrouc, L.: Comparison of nitrogen Monoxide emissions from several African tropical ecosystems and influence of season and fire, Global Biogeochem. Cycles, 12, 637–651, 1998.

Steinbacher, M., Zellweger, C., Schwarzenbach, B., Bugmann, S., Buchman, B., Ordóñez, C., Prevot, A. S. H., and Hueglin, C.: Nitrogen oxide measurements at rural sites in Switzerland: Bias of conventional measurement techniques, J. Geophys. Res.-Atmos., 112, D11307, doi:10.1029/2006JD007971, 2007.

Taylor, C. M., Saïd, F., and Lebel, T.: Interactions between the land surface and mesoscale rainfall variability during HAPEX-Sahel, Mon. Weather Rev., 125, 2211–2227, 1997.

Taylor, C. M., Ellis, R. J., Parker, D. J., Burton, R. R., and Thorncroft, C. D.: Linking boundary-layer variability with convection: A case-study from JET2000, Q. J. Roy. Meteorol. Soc., 129, 2233–2253, 2003.

Taylor, C. M., Parker, D. J., and Harris, P. P.: An Observational Case Study of Mesoscale Atmospheric Circulations Induced By Soil Moisture, Geophys. Res. Lett., 34, L15801, doi:10.1029/2007GL030572, 2007.

Watson, R. T., Meiro Filho, L. G., Sanhueza, E., and Jametos, A.: Greenhouse Gases: Sources and Sinks, in: Climate Change 1992 – The Supplementary Report to the IPCC Scientific Assessment, Houghton, J. T., Callande, B. A., and Varney, S. K., pp. 25–46, Cambridge, CUP, 1992.

Warneck, P.: Chemistry of the Natural Atmosphere, Academic Press, London, 1988.

Wayne, R. P.: Chemistry of Atmospheres 2nd Edition, Oxford University Press, 1991.

Yan, X., Ohara, T., and Akimoto, H.: Statistical Modelling of Global Soil NO$_x$ Emissions, Global Biogeochem. Cycles, 19 GB3019, doi:10.1029/2004GB002276, 2005.

Yienger, J. J. and Levy, H.: Empirical model of global soil-biogenic NO$_x$ emissions, J. Geophys. Res.-Atmos., 100, 11 447–11 464, 1995.